First-principles indicators of ferroic parameters in epitaxial BiFeO₃ and BiCrO₃

Cite as: J. Appl. Phys. **132**, 024102 (2022); https://doi.org/10.1063/5.0088121 Submitted: 21 February 2022 • Accepted: 16 June 2022 • Published Online: 11 July 2022

🗓 Michael R. Walden, 🗓 Cristian V. Ciobanu and 🗓 Geoff L. Brennecka







ARTICLES YOU MAY BE INTERESTED IN

Study on electrical activity of grain boundaries in silicon through systematic control of structural parameters and characterization using a pretrained machine learning model Journal of Applied Physics 132, 025102 (2022); https://doi.org/10.1063/5.0086193

Manifold learning and segmentation for ultrasonic inspection of defects in polymer composites

Journal of Applied Physics 132, 024901 (2022); https://doi.org/10.1063/5.0087202

Electrical spectroscopy methods for the characterization of defects in thin-film compound solar cells

Journal of Applied Physics 131, 240901 (2022); https://doi.org/10.1063/5.0085963

AIP

Journal of Applied Physics Special Topics Open for Submissions

First-principles indicators of ferroic parameters in epitaxial BiFeO₃ and BiCrO₃

Cite as: J. Appl. Phys. 132, 024102 (2022); doi: 10.1063/5.0088121

Submitted: 21 February 2022 · Accepted: 16 June 2022 ·

Published Online: 11 July 2022







Michael R. Walden, 1,a) (D) Cristian V. Ciobanu, 2 (D) and Geoff L. Brennecka 1 (D)

AFFILIATIONS

- Department of Metallurgical and Materials Engineering, Colorado School of Mines, Golden, Colorado 80401, USA
- ²Department of Mechanical Engineering, Colorado School of Mines, Golden, Colorado 80401, USA

ABSTRACT

Density-functional theory is used to validate spin-resolved and orbital-resolved metrics of localized electronic states to anticipate ferroic and dielectric properties of BiFeO₃ and BiCrO₃ under epitaxial strain. Using previous investigations of epitaxial phase stability in these systems, trends in properties such as spontaneous polarization and bandgap are compared to trends in atomic orbital occupation derived from projected density of states. Based on first principles theories of ferroic and dielectric properties, such as the Modern Theory of Polarization for spontaneous polarization or Goodenough–Kanamori theory for magnetic interactions, this work validates the sufficiency of metrics of localized electronic states to predict trends in multiple ferroic and dielectric properties. Capabilities of these metrics include the anticipation of the transition from G-Type to C-Type antiferromagnetism in BiFeO₃ under 4.2% compressive epitaxial strain and the interval of C-Type antiferromagnetism from 3% to 7% tensile epitaxial strain in BiCrO₃. The results of this work suggest a capability of localized electronic metrics to predict multiferroic characteristics in the BiXO₃ systems under epitaxial strain, with single or mixed B-site occupation.

Published under an exclusive license by AIP Publishing. https://doi.org/10.1063/5.0088121

I. INTRODUCTION

The bismuth-based perovskite oxides (BiXO₃, BXO) are stable in the absence of epitaxial strain in phases exhibiting many combinations of multiferroic behaviors. 1-4 Applications in energy harvesting, sensing, and computing require particular multiferroic characteristics to be stable under ambient conditions in a candidate material.⁵⁻¹² Although BiFeO₃ is the only BXO system exhibiting multiferroicity at room temperature, 13 B-site occupations by X = Cr, Mn, Ni, or Co associate with Curie or Néel temperatures of 100s of Kelvin, $^{13-18}$ prompting general interest in tuning for multiferroicity in the broader BXO compositional space with mixed B-site occupation. Phases stabilized in epitaxial thin films in the BiFeO₃ (BFO), BiCrO₃ (BCO), and BiMnO₃ systems (see Fig. 1) have been demonstrated to exhibit forms of multiferroicity not found in the unstrained BXO systems. 2,19-37 The dependence of multiferroicity in the BXO systems on composition and epitaxial strain may be explained through first principles theories expressing ferroic characteristics in terms of localized electronic states, as in the basis of spontaneous polarization in the bismuth 6s "lone pair" or the basis of B-site magnetic moment correlation in the oxygenmediated B-site interactions as analyzed by Goodenough and

Kanamori.^{38–47} No investigation known to the authors leverages localized electronic states for the prediction of ferroic or dielectric properties in the epitaxial BXO systems.

This work deals with ferromagnetism and ferroelectricity as separate, coexisting properties, and does not consider magnetoelectric coupling. Each ferroic and dielectric property investigated can be correlated to localized electronic states according to wellestablished first principles theories. The local electric dipole moments necessary for ferroelectricity (or antiferroelectricity) are stabilized relative to centrosymmetric phases by the stereochemical properties of the bismuth 6s lone electron pair. 54 The expression of this correlation between spontaneous polarization and localized electronic states is developed in the Wannier function basis in the Modern Theory of Polarization. 41 The correlation of magnetic moments of transition metal B-site cations (X in Fig. 1) resulting in antiferromagnetic or ferromagnetic order is mediated by superexchange interactions between B-site cations, as mediated by oxygen anions. 42-44,47 Various ab initio electronic structure theorems (Kohn-Sham, Mott, Janak, etc.) may be used to develop analytic expressions for electronic bandgap in terms of localized electronic orbitals.^{55–58} In each of these theories of ferroic and dielectric

a)Author to whom correspondence should be addressed: michaelwaldenetal@gmail.com

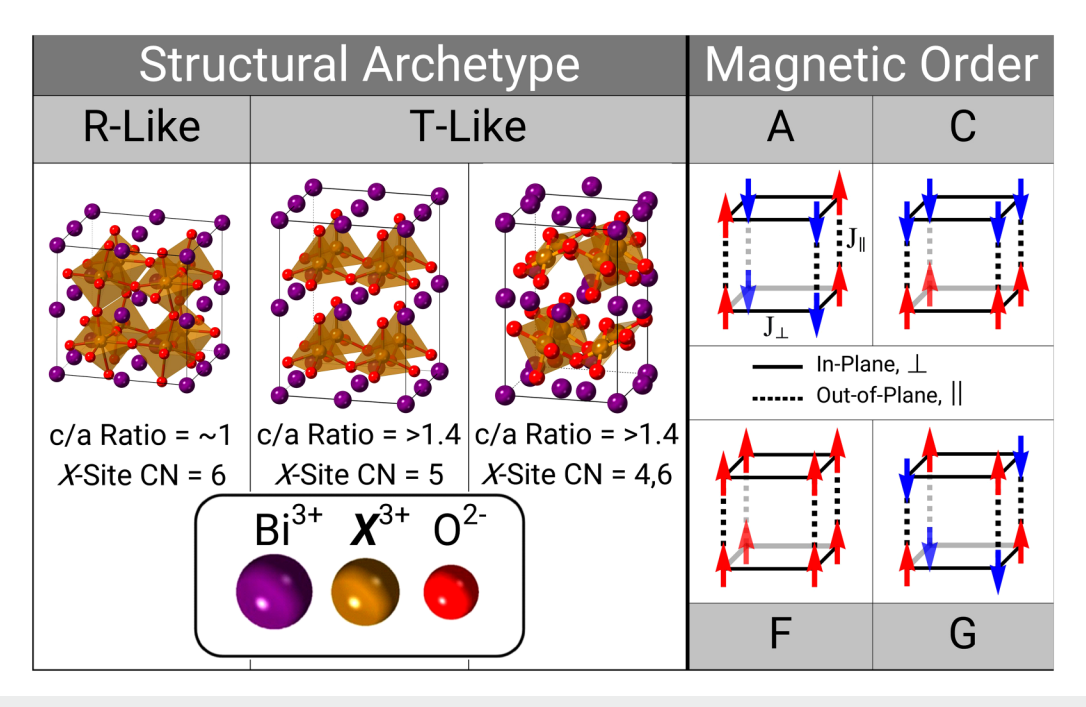


FIG. 1. Archetypes of structure and magnetic ordering in bismuth-based perovskite oxides. The rhombohedral-like (R-like) phases are common to most BXO systems, including BiFeO₃, BiCrO₃, and BiMnO₃. He two forms of tetragonal-like (T-like) phases illustrated indicate the presence of a tetragonal-elongation Jahn–Teller distortion. $^{14,51-53}$ The condition of fivefold B-site coordination corresponds to phases stable under ambient conditions in BiCoO₃ or under compressive epitaxial strain in BiFeO₃. 14,30,37,51 The condition of mixed fourfold/sixfold B-site coordination corresponds to phases stable under compressive epitaxial strain as in BiCrO₃. The illustrated magnetic orders presume first-neighbor, collinear correlation of B-site magnetic moments with degeneracy of coupling within the "in-plane" (IP, \perp) directions presumed to be nondegenerate with coupling perpendicular to this plane, in the direction denoted as "out-of-plane" (OP, \parallel).

properties, mathematical expressions for a given observable can be developed with functional dependence on some metric of localized electronic interactions. These interactions may be expressed in localized physical models through orbital overlap integrals or through site-projected electron field operators. The electronic density calculated with density-functional theory (DFT) methods may be transformed into spatially localized bases such as the Wannier function description or the crystal orbital overlap population (COOP) description. Post-processing software packages implementing these bases transformations on the outputs of DFT calculations include the "wannier90" and "LOBSTER" programs. We propose an alternative to these localized metrics of bonding electronic states which is more computationally efficient, while retaining a capability to screen for ferroic and dielectric properties in the bismuth-based perovskite oxides.

II. METHODOLOGY

A. Structural relaxation and ferroic property calculation

Using a similar approach as in our previous work,³⁷ we have carried out DFT calculations on the lowest-energy phases of BFO and BCO at a range of conditions of epitaxial strain. These calculations employ the generalized gradient approximation (GGA) as implemented in VASP,^{63–66} along with the

Perdew-Burke-Ernzerhoff (PBE) functional revised for solids (PBEsol).^{67,68} To correct for underestimation of electronic bandgap and other systematic errors pertaining to localized phenomena, our methods utilize the Dudarev implementation of Hubbard corrections for GGA (i.e., GGA+U).^{69,70} The Hubbard energy values, U, have been determined from the linearresponse method⁷¹ to be 4.6 eV for Fe and 4.8 eV for Cr, within the 0% epitaxial strain reference phases of BiFeO₃ and BiCrO₃. No significant variation in Hubbard energy is found in phases stabilized under non-zero epitaxial strain conditions, and these respective energy values are utilized uniformly in all calculations in this work. Calculations utilize a plane-wave energy cutoff of 540 eV and k-point grids of $5 \times 5 \times 5$ for dielectric/magnetic properties or $11 \times 11 \times 11$ for density of states (DOS) calculations. The valence electron configurations in our work are as follows: 6s²5d¹⁰6p³ for Bi, 3p⁶4s²3d⁶ for Fe, 3p⁶4s¹3d⁵ for Cr, and 2s²2p⁴ for O.

The ferroic and dielectric properties considered in this work include spontaneous polarization and bandgap, along with magnetic coupling coefficients calculated previously.³⁷ Spontaneous polarization calculations employ the Berry phase approach implemented in VASP,⁷² using discrete structure variations from 90% to 100% polar distortion to deconvolute the branching character of polarization.⁴¹ The Hubbard on-site energy is chosen as the sole method of correcting for the systematic underestimation of

bandgap in DFT methods, due to the high computational cost of GW-based corrections for equivalent accuracy in predicted bandgap energies⁵⁸ and due to previous reports that hybrid functional methods may overestimate bandgap in BXO systems.⁷³ Reported symmetry components of orbital occupation and spontaneous polarization may be reported in the Cartesian basis in which values in the VASP program are directly reported or in a simplified orthogonal basis spanned by "in-plane" (IP) and "out-of-plane" (OP) vectors defined in relation to the plane of (001) pc biaxial/epitaxial strain.

B. Orbital occupation and derived metrics

The atomic orbital occupations constituting the basic building blocks of this work are determined by numerically integrating the projected density of states (DOS) over all energies below the Fermi energy at which DOS is non-zero. This scheme yields spinpolarized orbital occupation resolved to each atomic site. The orbital resolution of this scheme references a Cartesian basis, which is aligned in our work with the pseudo-cubic perovskite lattice associated with the phases stable under (001) pc-oriented epitaxial strain in the BiFeO₃ and BiCrO₃ systems. The general alignment of the Cartesian orbital basis with the octahedral coordination of B-site cations by six oxygen anions is chosen due to the predominance of B-site cations in determining properties in the bismuthbased perovskite oxides. Though the bismuth cations are relevant to spontaneous polarization, the 12-fold coordination of the perovskite A-site by oxygen rules out simple associations of orbitals in a Cartesian basis with bismuth-oxygen bonding orbitals.

The site-, orbital-, and spin-resolution of tabulated occupation metrics must be treated independently, due to broken degeneracies resulting from spin-polarization, epitaxial strain, and out-of-phase rotation of first-nearest neighboring X-O octahedra. Our nomenclature follows the form: $N(Cr_i; d_z^2;)$, indicating the occupation of the ith chromium site in the d_{z^2} orbital and in the spin-up channel. Single-orbital metrics of this sort enable prediction of electronic bandgap. Multi-orbital products composed of two or four orbitals enable prediction of spontaneous polarization and magnetic order. A simple example of a two-orbital product is the strength of a chemical bond, parameterized by the product of two occupations metrics corresponding to symmetry- and spin-permissible combinations of orbitals on first-neighboring atomic sites. The strength of a Cr–O chemical bond generally aligned with the $[001]_{pc}$ axis (z-axis, in the Cartesian basis) may be parameterized as

$$N_2(Cr_i-O_j;z) = N(Cr_i; d_{z^2}; /), : N(O_j; p_z; /).$$
 (1)

In this notation, the *i*th Cr site is presumed to be a first-nearest neighbor of the *j*th O site along the $[001]_{pc}$ pseudo-cubic axis. This notation implies a summation over both spin combinations, though each combination of Cr–O sites which are first-nearest neighboring will in general be treated separately, due to the possible non-equivalence of atomic sites of the same species except when enforced by periodic boundary conditions.

These two-orbital metrics may be further refined in spinpolarized pairs as four-orbital metrics associating with the superexchange interaction between two first-nearest B-site neighbors, as

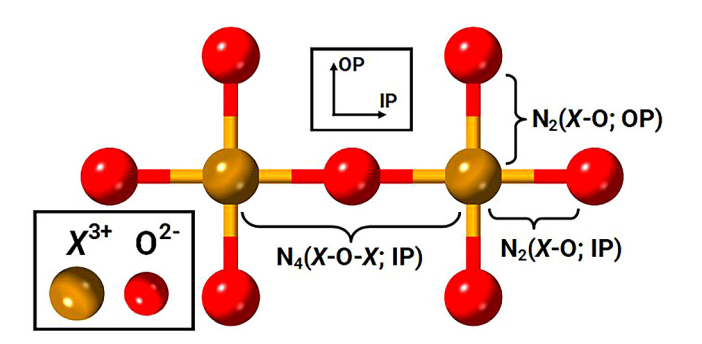


FIG. 2. Illustration of two- and four-orbital occupation syntax.

mediated by an immediately intervening O site. These metrics, as illustrated in Fig. 2, utilize the following syntax following the pattern of Eq. (1):

$$N_4(Cr_i-O_i-Cr_k; z) = N_2(Cr_i-O_i; z), : N_2(Cr_k-O_i; z).$$
 (2)

These localized orbital occupation metrics do not explicitly consider orbital overlap. Our localized metrics, therefore, are less accurate than those of the LOBSTER or wannier90 methods and may not accurately predict the magnitudes of ferroic or dielectric properties in a particular material system. However, we propose that our metrics, being fundamentally derived from one-site/one-orbital occupations, are a simple and computationally efficient alternative to multi-site/multi-orbital metrics, due to the greater independence of one-site terms from the first-neighboring, second-neighboring, etc. coordination environment. Our metrics may, therefore, enable rapid screening for ferroic and coupled multiferroic properties within material spaces containing large crystal structure sets or large compositional ranges.

III. RESULTS/DISCUSSION

A. Dependence of orbital occupation on epitaxial phase stability

The ranges of spin-polarized and orbital-resolved occupations calculated to be stable under the considered range of epitaxial strain are listed in Table I. The total occupation of all orbitals in all atomic sites in a modeled formula unit of BFO ranges from 39.70 to 40.35 and for BCO from 38.11 to 39.27. The valence electronic configurations employed correspond, respectively, to 47 and 45 electrons per formula unit in these systems. These discrepancies are in part attributable to deviation in charge density from the tightbinding model, which presumes that charge density in a crystal may be sufficiently described in terms of linear combinations of orbitals localized near each crystallographic site in the modeled supercell. Insofar as this model is applicable, any changes under epitaxial strain in orbital occupation for a given atomic species should be conserved. For instance, the stabilization of T-like phases in BFO under moderate compressive epitaxial strain leads to stronger Fe-O bonds within the epitaxial plane and weaker bonds perpendicular to this plane, suggesting a generally conserved shift in

TABLE I. Range of variation in BXO atomic orbital occupation under epitaxial strain, contrasted with integer initialized valence shell configuration.

System	Atom	Orbital	Initial	Occupations
BFO	Bi	S	2	1.61-1.64
		p	3	0.85-0.92
		d	10	10.02-10.06
	Fe	s	2	0.30-0.35
		p	6	6.37-6.47
		d	6	5.64-5.79
	O	S	2	1.56-1.57
		p	4	3.41-3.47
ВСО	Bi	s	2	1.60-1.68
		p	3	0.80 - 0.93
		d	10	9.98-10.02
	Cr	S	1	0.36 - 0.44
		p	6	6.57-6.80
		d	5	4.01-4.31
	O	S	2	1.55-1.56
		p	4	3.38-3.47

population of the Fe d_{z^2} orbital toward the $d_{x^2-y^2}$ orbital under increasing compressive epitaxial strain. This intuition is confirmed in Fig. 3, illustrating the trends with epitaxial strain in key atomic orbital occupation metrics.

An additional contribution to the discrepancy between the occupations in Table I and the integer valence configurations is the mismatch between interatomic spacings and Wigner-Seitz radii. In the 0% strain (bulk) condition, the lowest-energy phases of the BFO and BCO systems calculated in our work have pseudo-cubic lattice constants of 3.95 and 3.90 Å, respectively. These conditions lead to interatomic Bi-O spacings of 2.76-2.79 Å, Fe-O spacings of 1.98 Å, and Cr-O spacings of 1.95 Å. The sums of Wigner-Seitz radii used in our calculations are, for these respective atomic pairs, 2.46, 2.14, and 1.98 Å. The deviation is greatest for the Bi-O atomic pairs, suggesting errors in accounting for these bonding interactions. The use of our atomic orbital occupation metrics for Bi-O interactions is further sub-optimal due to the 12-fold coordination of bismuth by oxygen. Whereas in the X-O octahedral coordination environment, vectors between bonding atomic pairs may be generally aligned with the atomic orbitals as projected in the VASP code into a Cartesian basis, no such convenience is possible in the Bi-O coordination environment. Consideration of some Bi-O interaction aligned with the $[110]_{pc}$ crystallographic axis, for instance, may require N₂ metrics considering the p_r and p_v orbitals of both bismuth and oxygen. Because the only ferroic or dielectric property associated in common first principles theories with localized states of bismuth is the dependence of spontaneous polarization on the bismuth lone-pair, we exclude from consideration any N₂ metrics associating with both bismuth orbitals and orbitals of neighboring oxygen sites and utilize only "on-site" occupation metrics for bismuth.

As illustrated in Fig. 3, the bismuth s/p-orbital states vary in occupation significantly under epitaxial strain in both the BFO and BCO systems. However, the bismuth d-orbital occupation remains

essentially at the integer 10 occupation at all strain conditions. This result suggests that DFT calculations of the BXO systems may consider the bismuth 5d states as core rather than valence with no meaningful decrease in accuracy. All other occupations differ nonnegligibly from the initial/uncharged integer values. We emphasize the absence of principal quantum number denotations beyond the consideration of core and valence electronic states. The projected DOS values are calculated as the overlap of Bloch wavefunctions with the site-localized spherical harmonics. Radial character of these orbital occupations arises only through the Wigner–Seitz radii. No conditions of orthonormality are violated by the occupation of B-site cation p-orbitals by greater than six electrons. However, the presumption that only 10 electronic states are available to d-orbital states is useful in a qualitative sense to use trends in B-site coordination symmetry to justify trends in B-site d-orbital occupation.

The trends in B-site orbital occupation illustrated in Figs. 3(c)-3(f) describe the d_{xy} , d_{yz} , and d_{zx} orbitals separately from the $d_{x^2-y^2}$ and d_{z^2} orbitals. We refer in Fig. 3 and in the remainder of this work to these two classifications of d-orbital states as "planar" and as "axial," respectively, in keeping with the IP/OP nomenclature (illustrated in Fig. 1) common in the literature on epitaxial BXO systems. The axial nomenclature for d-orbital states refers to the association of lobes with the Cartesian axes such that these states may be expected to contribute more than planar orbitals to bonding between B-site cations and octahedrally coordinate oxygen anions. Analysis of this coordination environment from a crystal field theoretic perspective may be immensely useful in further developments of the utility of metrics of localized electronic states beyond the scope of this work. However, this work shows that analysis of the coordinate symmetry at a general, qualitative depth is sufficient for prediction of trends with epitaxial strain in ferroicity. For instance, the discontinuous drop in d_{xy} occupation in BFO at the transition from G-Type to C-Type phases under compressive epitaxial strain shown in Fig. 3(c) is consistent with the $a^0a^0c^0$ Glazer notation of T-like phases with fivefold B-site coordination, as illustrated in Fig. 1. Quantitative determination of the d-orbital splitting energies stabilizing this specific coordination environment is beyond the scope of this work.

B. Associating orbital occupation with ferroicity

The mechanisms associating localized electronic states with ferroic and dielectric characteristics in the BXO systems are well-established on a theoretical basis. ^{41-47,54,58} For instance, phase stability in structures that are locally non-centrosymmetric at the level of individual perovskite formula units, permitting either ferroelectricity or antiferroelectricity in the BXO systems, ^{14,16,74-84} has been well established to associate with the stereochemical properties of the bismuth 6s lone-pair. ⁵⁴ The wide range of combinations of ferroic properties (ferro-, antiferro-, ferri-; electric, magnetic, elastic) associated with the epitaxial BXO material space indicates that multiferroicity is determined uniquely by the valence electronic configuration and coordination environment of the B-site cation(s). Though mechanisms for coupled multiferroicity (magnetoelectricity) may be developed through the Dzaloshinskii–Moriya interaction, ⁴⁷ this work considers only the individually ferroic properties given by the aforementioned mechanisms. To the degree that the on-site and nearest-neighboring

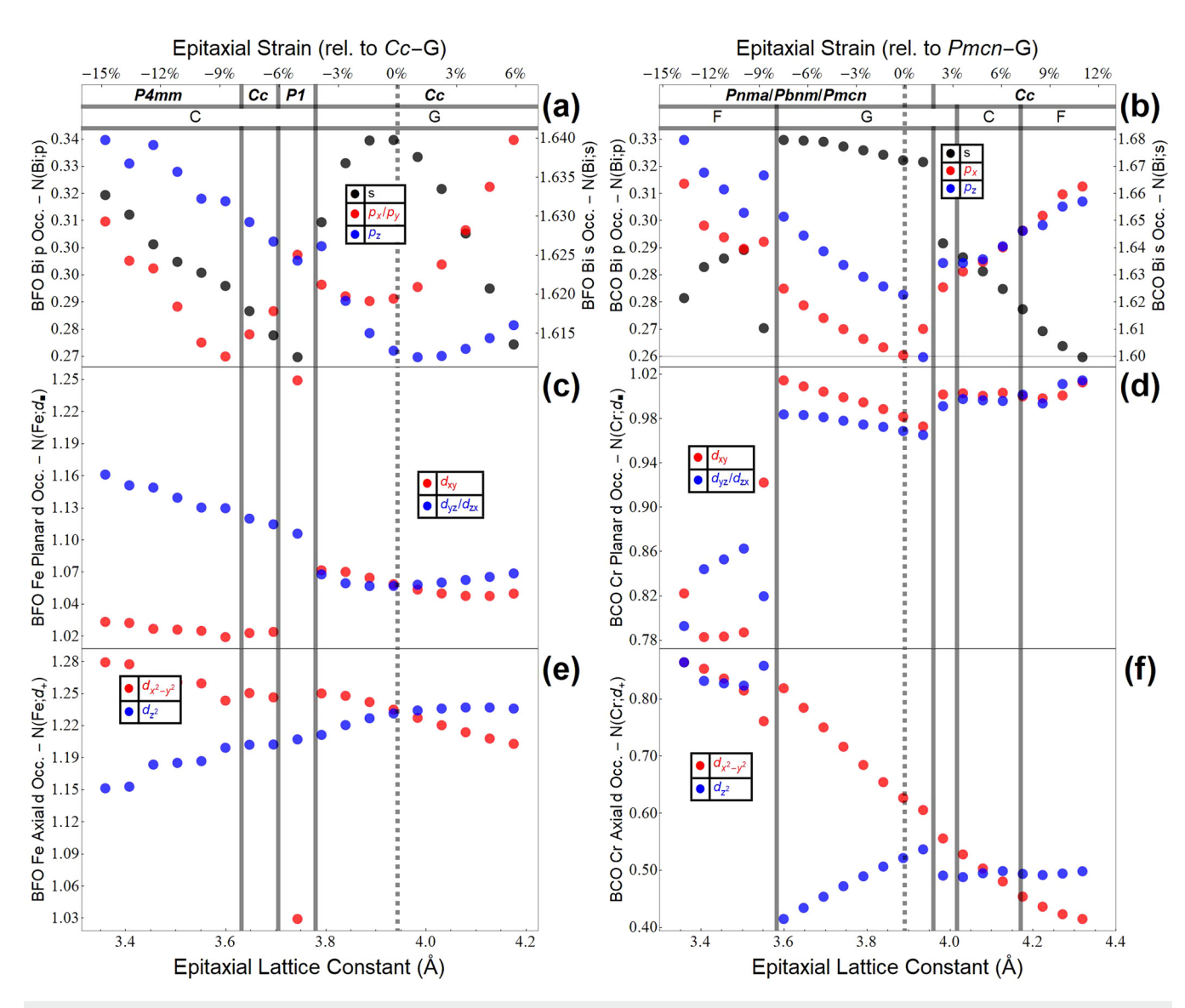


FIG. 3. Variation with epitaxial strain of total occupation in significant cation orbitals in the BFO [(a), (c), (e)] and BCO [(b), (d), (f)] systems, under epitaxial strain. The top banner on panels (a) and (b) indicates the space group (e.g., *P4mm*, *Pnma*, *Cc*, etc.) and magnetic order (G-, C-, or F-Type), which is the lowest energy in each region of epitaxial strain. Epitaxial strain is given in both absolute values (Å) and relative to the global energy minimum phase in each system (%), which is G-Type magnetic order and the *Cc* space group in BFO and G-type magnetic order and the *Pmcn* space group in BCO. More information on these structures and magnetic orders is given in our prior work.

interactions of B-site cations with the BXO lattice are sufficient to predict the coexistence of multiple ferroic properties in the single-perovskite BXO systems, we propose that these metrics are likewise sufficient to predict coupled multiferroicity in the mixed-perovskite BXO systems, such as Bi(Fe,Cr)O₃.

C. Identification of BCO orbital occupations contributing to bulk ferroic, dielectric properties

Though the first principles theories we have cited previously set well-defined combinations of orbitals associating with ferroic and dielectric properties in the BXO systems, some ambiguous characteristics remain. For instance, given the various spin-polarized (anti-)ferromagnetic states that may be stable in the BFO and BCO systems, the spin-up channel, the spin-down channel, or some combination of both channels may be most strongly associated with some ferroic property. The focus on BFO in the literature reports on epitaxial BXO multiferroicity leads to the choice to develop our proposed occupation metrics for the BCO system first, and only then to determine generality/transferability to BFO.

1. Contributions to bandgap in BCO from Cr $\rm d_{z^2}$ occupation

Bandgap in the BFO and BCO systems generally falls in the range of 1.7-2.0 eV if the gap is indirect or 2.5-2.7 for direct ^{9–92} The influence of epitaxial strain on bandgap is mediated by the symmetry of the B-site coordination environment, with lower degrees of anti-phase rotation (as in T-like BFO) associating with decreasing bandgap.⁹³ Analysis of the spin-resolved electronic band structure of BCO indicates that the maximum energy of the valence band is associated with the spin-down channel of the d_{z^2} orbital. The trends in this orbital occupation and in the bandgap with epitaxial strain in the BCO system are shown in Figs. 4(b) and 4(d). The occupation trend is bimodal in the regime of G-Type magnetic order, with the greater occupation value more closely following the trend in bandgap. Comparison of these trends shows a significant quantitative capability for bandgap prediction, both within regimes of phase stability and through discontinuities associated with phase transitions. Most notable is the vanishing occupation and bandgap associated with the at least 8% compressive epitaxial strain. Confident prediction of epitaxial strain regimes where bandgap would be expected to vanish, leading to conductive character, is a significant capability of these metrics.

This vanishing bandgap at the G-Type to F-Type magnetic transition under compressive strain corresponds to a transition from sixfold Cr–O coordination to a disordered T-like phase. As has been explored in part in our prior work,³⁷ this is a structurally non-parsimonious phase exhibiting an even mixture of fourfold and sixfold Cr–O coordination. The significant conductive character of this phase is problematic in DFT calculations, which may exhibit charge sloshing or other forms of non-equilibrium in systems. The DFT methods we have used do not permit calculation of spontaneous polarization in this strain regime.

2. Contributions to spontaneous polarization in BCO from Bi s/p-orbital occupation

We find the orthorhombic phases in which the BCO system is stable under compressive epitaxial strain to be uniformly centrosymmetric, therefore exhibiting zero spontaneous polarization in this strain regime. Our methods do not permit distinguishing antiferroelectricity or simply non-ferroelectricity, though locally antialigned electric dipole moments are present. The general invariance in occupation of the spherical s-orbital states in bismuth shown in Fig. 3(b) within the G-Type orthorhombic regime of phase stability, compared to other phase regimes within BCO or BFO, may be an

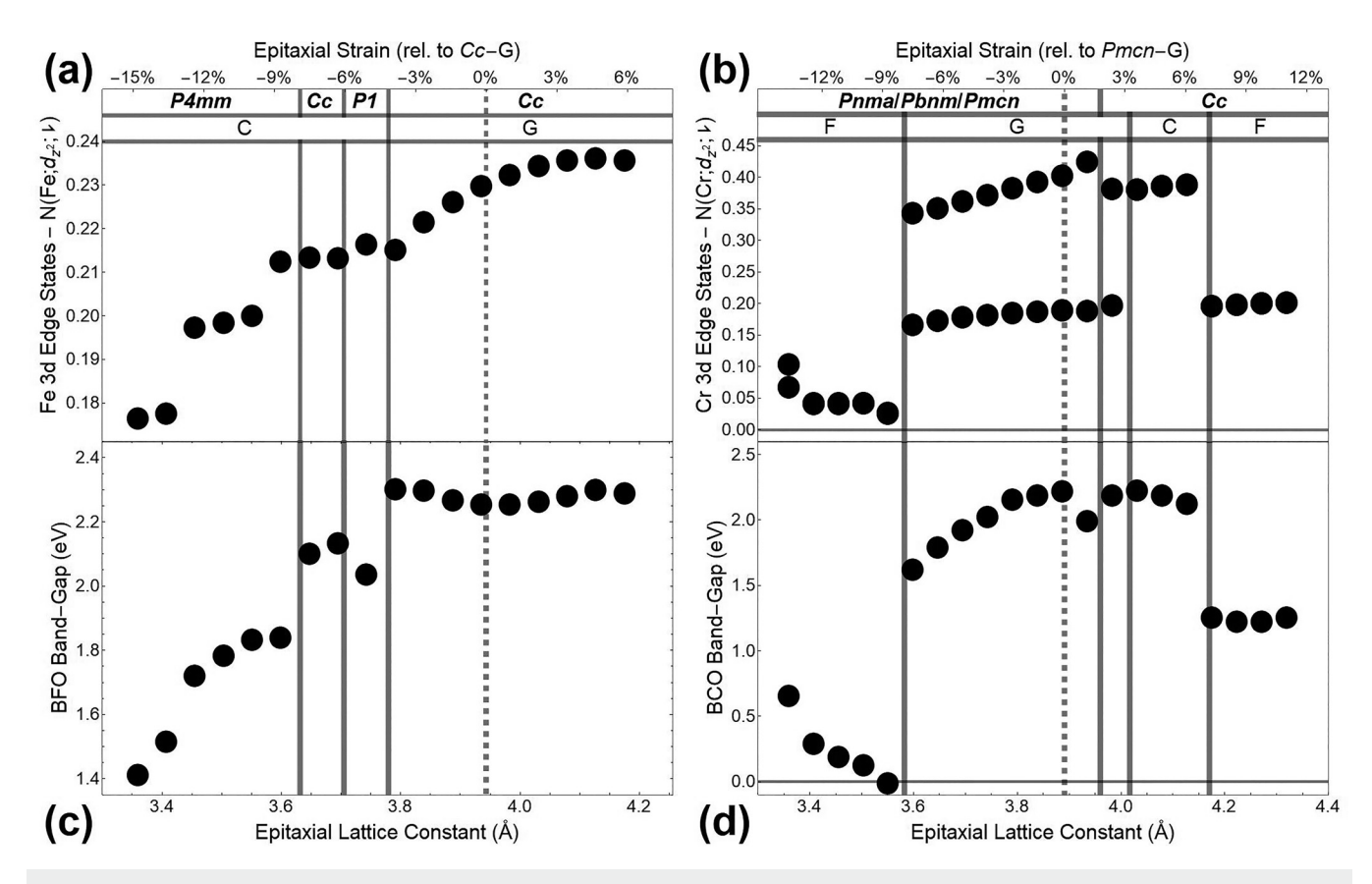


FIG. 4. Variation with epitaxial strain of the proportion of B-site d-orbital occupation associated with the d_{z^2} orbital in the BFO (a) and BCO (b) systems and of the bandgap of the BFO (c) and BCO (d) systems.

indicator of centrosymmetry. Analysis of other BXO systems, such as BiMnO₃, could increase confidence in this qualitative association. In the BCO phase under tensile strain, the s/p-orbital occupations of bismuth vary continuously and trivially. The known trend in spontaneous polarization orientation from the $[111]_{pc}$ axis toward the $[110]_{pc}$ under increasing compressive epitaxial strain in any BXO system is a trivial inference from this occupation trend. The centrosymmetry under compressive strain and trivial variation in spontaneous polarization under tensile strain in the BCO system does not permit strong confidence in the capability of the s/p-orbital occupation metrics to quantitatively predict spontaneous polarization.

Contributions to magnetic order in BCO from Cr-O-Cr four-orbital occupation products

The superexchange basis of magnetic correlation is the subject of theoretical analysis by Goodenough and Kanamori, which includes the development using second-order perturbational theory of an analytic expression for the collinear, Heisenberg-like coupling coefficient between first-neighboring B-site cations explicitly incorporating the orbital overlap between each B-site cation, and the oxygen anion immediately mediating between those cation sites. 42-44 The trends with epitaxial strain in the four-orbital occupation metrics associated with these superexchange interactions are shown in Fig. 5(b). The uniform character of these metrics is surprising, given the significant changes in B-site d-orbital and oxygen p-orbital occupations shown in Figs. 3(b) and 3(f). This invariance except at transitions between antiferromagnetic orders suggests a direct relationship between these N₄ metrics and sign but not magnitude of collinear, first-neighboring magnetic coupling coefficients. These coefficients, as calculated in our prior work,³⁷ vary significantly and discontinuously at magnetic phase transitions in the BFO and BCO systems. The parameters in the Goodenough-Kanamori analysis that determine the magnitude of magnetic coupling coefficients may be the Hubbard-like on-site energies and one-electron orbital energies. Though we calculate on-site energies using *ab initio* linear response methods in order to improve calculation of localized electronic properties like bandgap, we do not consider one-electron orbital energies. As has been stated previously, such considerations would require a crystal field theoretic analysis of the B-site cations, which is beyond the scope of this work. Rather, we limit the scope of this work to determine the capability of the patterns in N_4 metrics shown in Fig. 5(b) to anticipate stable magnetic order under epitaxial strain. Because magnetic order depends solely on the relative alignment of neighboring B-site magnetization vectors and not on the magnitude of those vectors, we refer to our previous work for the dependence of magnetization in the BFO and BCO systems on epitaxial strain.³⁷

The region of G-Type stability in Fig. 5(b) associates with both IP and OP N₄ metrics being generally equal in magnitude, separated bimodally into a value near to zero and some definitively non-zero value. G-Type stability is characterized by anti-parallel correlation of B-site moments in both the IP and OP directions. We find in the regions of C-Type and F-Type stability in BCO under tensile epitaxial strain that the bimodal separation of N₄ values for the IP and OP axes reduces to a singular value in exactly those orientations, which correspond to alignment of B-site moments (OP in C-Type, IP+OP in F-Type). The comparability of bimodal IP N₄ magnitude in both the G-Type orthorhombic phase under compressive strain and the C-Type monoclinic phase under tensile strain is remarkable, given the significant structural differences between these phases. Even the structurally non-parsimonious F-Type orthorhombic phase shows some comparability to the C-Type and F-Type monoclinic phases. This high-compression phase exhibits two values of the OP N₄ metric, even though the previously outlined logic would suggest that F-Type stability should correspond to a singular value. However, this high-compression phase exhibits a mixture of fourfold and sixfold B-site coordination, as illustrated in Fig. 1. The greater magnitude of the N₄ metric is found to correspond to the sixfold coordinated

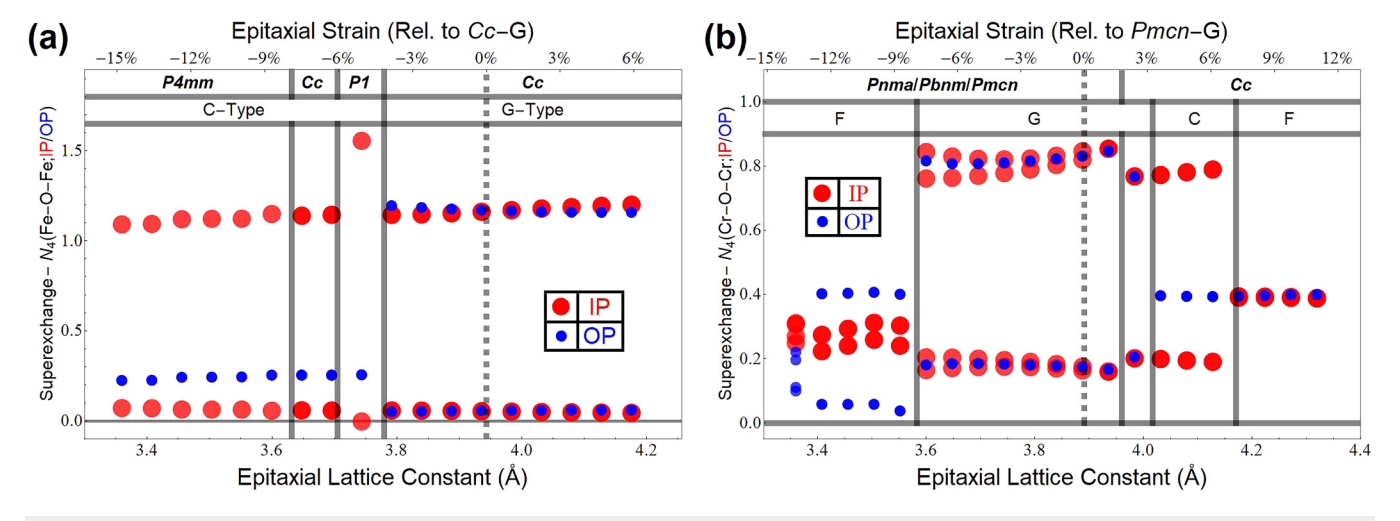


FIG. 5. Variation with epitaxial strain of IP and OP N₄ occupation products in the BFO (a) and BCO (b) systems.

chromium sites, with the fourfold coordinated sites corresponding to the lower value.

D. Translation of BCO electronic mechanisms to the BFO system

1. Bandgap mechanism in BFO

The B-site $\rm d_{z^2}$ spin-down occupation is shown in Figs. 4(a) and 4(c) to enable prediction of bandgap trends with epitaxial strain in the BFO system. As in the BCO system, discontinuities in bandgap at phase transitions are largely reflected in the occupation metrics as well. The relative magnitudes of the occupation metrics are consistent with the uniform insulating character of the BFO system across the entire considered epitaxial strain range, leading to compatibility of our DFT methods with calculation of spontaneous polarization in all phase regimes. The transition to T-like stability beyond \sim 4.2% compressive epitaxial strain as expected leads to a decrease in bandgap, but the uniform fivefold coordination of iron sites by oxygen without the non-parsimonious structures associated with BCO under high compressive strain is consistent with this general insulating character.

2. Spontaneous polarization mechanism in BFO

The BFO system exhibits uniform non-centrosymmetry and non-trivial variation in spontaneous polarization, permitting evaluation of bismuth s/p-orbital occupation metrics as predictors of spontaneous polarization. The "on-site" N2 metrics involving IP/OP symmetrized pairs of s-orbital and p-orbital states show in Fig. 6 trends with epitaxial strain consistent with the orientation of spontaneous polarization in BFO. The trends within the Cc monoclinic phase are somewhat trivial given the continuity of this phase with the R3c phase stable in BFO in the unstrained condition. The vanishing IP component of spontaneous polarization across the transition from R-like to T-like character, due to the shift in orientation from the $[111]_{pc}$ to the $[001]_{pc}$ axis, is consistent with the significant drop in IP s/p-orbital occupation relative to OP sp occupation. The decrease in spontaneous polarization within the C-Type region of P4mm stability predicted in our work corresponds to a region of epitaxial strain not known to the authors have been investigated computationally or experimentally in the BFO system. The maintenance of spontaneous polarization in the 90–100 μ C/cm² interval within the region of *P4mm* stability may perhaps be anticipated due to the near equivalence of slopes in the IP and OP s/p-orbital occupation metrics within this phase. Analysis of the ionic and electronic contributions to spontaneous polarization within this high-compression regime shows almost exactly offsetting increases in both under increasing compressive epitaxial strain.

3. Magnetic correlation mechanism in BFO

The four-orbital metrics for superexchange transfer exactly from the BCO system to the BFO system. The association of bimodal N_4 metrics with B-site moment anti-alignment and single-valued metrics with moment alignment holds exactly. Only the P1 monoclinic phase is associated with a meaningful deviation from the invariance in these N_4 metrics under epitaxial strain.

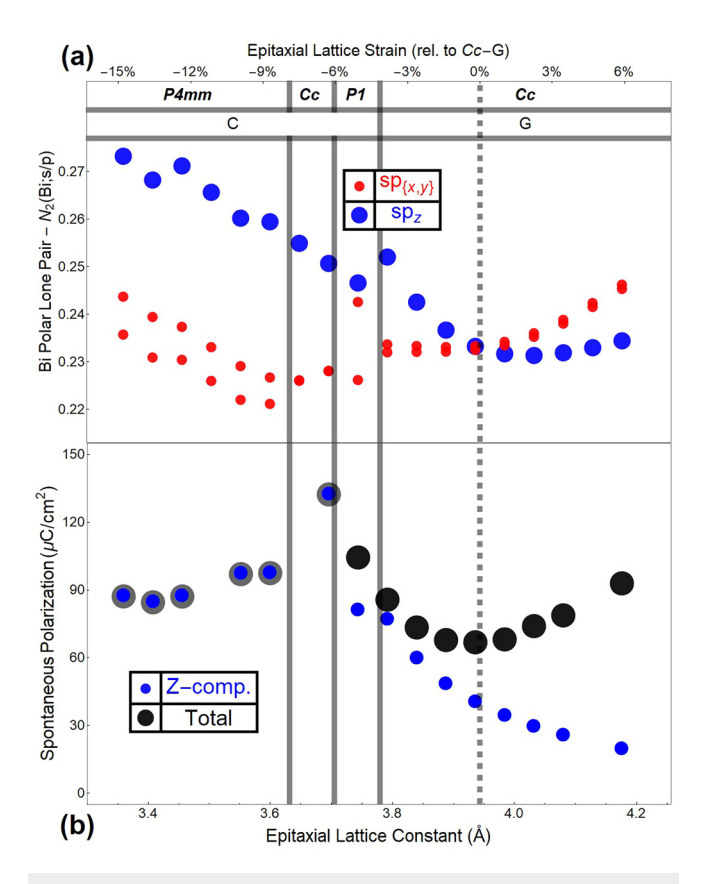


FIG. 6. Variation with epitaxial strain of the products on a given bismuth site of the s- and p-orbital occupations in the BFO system (a); the overall magnitude of spontaneous polarization and the component of spontaneous polarization along the [001] crystallographic direction in the BFO system (b).

No variation in the N_4 metrics is sufficient to account for the variation in magnitude of magnetic coupling coefficients calculated in our prior work.³⁷

IV. CONCLUSIONS

This work demonstrates a strong association of atomic orbital occupation metrics with trends in ferroic and dielectric properties in the BiFeO₃ and BiCrO₃ systems under a wide range of epitaxial strain. These associations include the capability to predict quantitatively the trends with epitaxial strain in bandgap and spontaneous polarization and may even enable anticipation of stability of centrosymmetric phases. We propose metrics enabling prediction of stable antiferromagnetic order and suggest that no metric of localized electronic states without augmentation by other on-site parameter trends with epitaxial strain can predict quantitative trends in magnetic coupling coefficients. We theorize that the A-site and B-site sublattices in an ABO₃ framework may be treated independently for the purposes of screening for ferroicity, provided proper accounting for the influence of relative A-site/B-site valences is considered. The steps taken to ensure generality and transferability

of occupation metrics to both the BFO and BCO systems support the objective of this work to develop metrics useful in prediction of multiferroicity in the mixed-perovskite BXO systems, such as Bi (Fe,Cr)O₃, under epitaxial strain. The influence of cation substitutions, as in ferroelectricity under non-bismuth substitution on the A-site sublattice or in ferromagnetism under non-trivalent substitution on either the A-site or B-site sublattices, represent natural extensions of our work to the more general ABO₃ multiferroic space beyond the bismuth-based perovskite oxides.

ACKNOWLEDGMENTS

M.R.W. was supported by a CoorsTek Research Fellowship through the Colorado School of Mines Foundation. G.L.B. and C.V.C. were supported in part by the National Science Foundation through Grant Nos. DMR-1555015 and DMREF-1629026, respectively.

AUTHOR DECLARATIONS

Conflict of Interest

The authors have no conflicts to disclose.

Author Contributions

Michael R. Walden: Methodology (lead); Investigation (lead); Writing - original draft (equal); Writing - review and editing (equal). Cristian V. Ciobanu: Methodology (supporting); Supervision (equal); Writing - original draft (equal); Writing - review and editing (equal). Geoff L. Brennecka: Investigation (supporting); Supervision (equal); Writing - original draft (equal); Writing - review and editing (equal).

DATA AVAILABILITY

The data that support the findings of this study are available from the corresponding author upon request.

REFERENCES

- G. D. Achenbach, W. J. James, and R. Gerson, "Preparation of single-phase polycrystalline BiFeO₃," J. Am. Ceram. Soc. 50, 437 (1967).
 I. C. Infante, J. Juraszek, S. Fusil, B. Dupé, P. Gemeiner, O. Diéguez, F. Pailloux,
- L. C. Infante, J. Juraszek, S. Fusil, B. Dupé, P. Gemeiner, O. Diéguez, F. Pailloux, S. Jouen, E. Jacquet, G. Geneste, J. Pacaud, J. Íñiguez, L. Bellaiche, A. Barthélémy, B. Dkhil, and M. Bibes, "Multiferroic phase transition near room temperature in BiFeO₃ films," Phys. Rev. Lett. 107, 237601 (2011).
- ³F. Kubel and H. Schmid, "Structure of a ferroelectric and ferroelastic monodomain crystal of the perovskite BiFeO₃," Acta Crystallogr., Sect. B: Struct. Sci. **46**, 698–702 (1990).
- ⁴X. Xi, S. Wang, W. Liu, H. Wang, F. Guo, X. Wang, J. Gao, and D. Li, "Enhanced magnetic and conductive properties of Ba and Co co-doped BiFeO₃ ceramics," J. Magn. Magn. Mater. **355**, 259–264 (2014).
- ⁵H. S. Kim, J.-H. Kim, and J. Kim, "A review of piezoelectric energy harvesting based on vibration," Int. J. Precis. Eng. Manuf. 12, 1129–1141 (2011).
- ⁶T. Hemsel and J. Wallaschek, "Survey of the present state of the art of piezoelectric linear motors," Ultrasonics 38, 37–40 (2000).
- ⁷J. F. Tressler, S. Alkoy, and R. E. Newnham, "Piezoelectric sensors and sensor materials," J. Electroceram. 2, 257–272 (1998).
- ⁸G. J. Snyder, "Thermoelectric energy harvesting," in *Energy Harvesting Technologies* (Springer US, Boston, MA, 2009), pp. 325–336.

- ⁹U. Dürig, "Fundamentals of micromechanical thermoelectric sensors," J. Appl. Phys. 98, 044906 (2005).
- 10 L. E. Bell, "Cooling, heating, generating power, and recovering waste heat with thermoelectric systems," Science 321, 1457–1461 (2008).
- ¹¹G. Sebald, D. Guyomar, and A. Agbossou, "On thermoelectric and pyroelectric energy harvesting," Smart Mater. Struct. 18, 125006 (2009).
- 12M. H. Lee, R. Guo, and A. S. Bhalla, "Pyroelectric sensors," J. Electroceram. 2, 229–242 (1998).
- ¹³P. Fischer, M. Polomska, I. Sosnowska, and M. Szymanski, "Temperature dependence of the crystal and magnetic structures of BiFeO₃," J. Phys. C: Solid State Phys. **13**, 1931–1940 (1980).
- ¹⁴A. A. Belik, S. Iikubo, K. Kodama, N. Igawa, S.-I. Shamoto, S. Niitaka, M. Azuma, Y. Shimakawa, M. Takano, F. Izumi, and E. Takayama-Muromachi, "Neutron powder diffraction study on the crystal and magnetic structures of BiCoO₃," Chem. Mater. 18, 798–803 (2006).
- 15A. A. Belik, "Magnetic properties of solid solutions between BiCrO₃ and BiGaO₃ with perovskite structures," Sci. Technol. Adv. Mater. 16, 026003 (2015).
 16F. Sugawara, S. Iiida, Y. Syono, and S.-I. Akimoto, "Magnetic properties and crystal distortions of BiMnO₃ and BiCrO₃," J. Phys. Soc. Jpn. 25, 1553–1558 (1968).
- ¹⁷I. V. Solovyev and Z. V. Pchelkina, "Magnetic ground state and multiferroicity in BiMnO₃," JETP Lett. **89**, 597–602 (2009).
- ¹⁸I. V. Solovyev, "Magnetic structure of the noncentrosymmetric perovskites PbVO₃ and BiCoO₃," Phys. Rev. B 85, 054420 (2012).
- ¹⁹H. M. Christen, J. H. Nam, H. S. Kim, A. J. Hatt, and N. A. Spaldin, "Stress-induced R- M_A - M_C -T symmetry changes in BiFeO₃ films," Phys. Rev. B 83, 144107 (2011).
- 83, 144107 (2011).
 20C. Daumont, W. Ren, I. C. Infante, S. Lisenkov, J. Allibe, C. Carrétéro, S. Fusil, E. Jacquet, T. Bouvet, F. Bouamrane, S. Prosandeev, G. Geneste, B. Dkhil, L. Bellaiche, A. Barthélémy, and M. Bibes, "Strain dependence of polarization and piezoelectric response in epitaxial BiFeO₃ thin films," J. Phys.: Condens. Matter 24, 162202 (2012).
- 21 B. Dupé, I. C. Infante, G. Geneste, P.-E. Janolin, M. Bibes, A. Barthélémy, S. Lisenkov, L. Bellaiche, S. Ravy, and B. Dkhil, "Competing phases in BiFeO₃ thin films under compressive epitaxial strain," Phys. Rev. B 81, 144128 (2010).
- ²²B. Dupé, S. Prosandeev, G. Geneste, B. Dkhil, and L. Bellaiche, "BiFeO₃ films under tensile epitaxial strain from first principles," Phys. Rev. Lett. **106**, 237601 (2011).
- ²³C. Escorihuela-Sayalero, O. Diéguez, and J. Íñiguez, "Strain engineering magnetic frustration in perovskite oxide thin films," Phys. Rev. Lett. 109, 247202 (2012).
- ²⁴A. J. Hatt, N. A. Spaldin, and C. Ederer, "Strain-induced isosymmetric phase transition in BiFeO₃," Phys. Rev. B **81**, 054109 (2010).
- ²⁵C. W. Huang, Y. H. Chu, Z. H. Chen, J. Wang, T. Sritharan, Q. He, R. Ramesh, and L. Chen, "Strain-driven phase transitions and associated dielectric/piezoelectric anomalies in BiFeO₃ thin films," Appl. Phys. Lett. **97**, 152901 (2010).
- ²⁶M. N. Iliev, M. V. Abrashev, D. Mazumdar, V. Shelke, and A. Gupta, "Polarized Raman spectroscopy of nearly tetragonal BiFeO₃ thin films," Phys. Rev. B 82, 014107 (2010).
- ²⁷I. C. Infante, S. Lisenkov, B. Dupé, M. Bibes, S. Fusil, E. Jacquet, G. Geneste, S. Petit, A. Courtial, J. Juraszek, L. Bellaiche, A. Barthélémy, and B. Dkhil, "Bridging multiferroic phase transitions by epitaxial strain in BiFeO₃," Phys. Rev. Lett. 105, 057601 (2010).
- ²⁸D. H. Kim, H. N. Lee, M. D. Biegalski, and H. M. Christen, "Effect of epitaxial strain on ferroelectric polarization in multiferroic BiFeO₃ films," Appl. Phys. Lett. 92, 012911 (2008).
- 29 K. Saito, A. Ulyanenkov, V. Grossmann, H. Ress, L. Bruegemann, H. Ohta, T. Kurosawa, S. Ueki, and H. Funakubo, "Structural characterization of BiFeO₃ thin films by reciprocal space mapping," Jpn. J. Appl. Phys. 45, 7311–7314 (2006).
 30 D. Sando, A. Barthélémy, and M. Bibes, "BiFeO₃ epitaxial thin films and devices: Past, present and future," J. Phys.: Condens. Matter 26, 473201 (2014).

- 31D. G. Schlom, L.-Q. Chen, C.-B. Eom, K. M. Rabe, S. K. Streiffer, and J.-M. Triscone, "Strain tuning of ferroelectric thin films," Annu. Rev. Mater. Res.
- 32S. M. Selbach, T. Tybell, M.-A. Einarsrud, and T. Grande, "Structure and properties of multiferroic oxygen hyperstoichiometric $BiFe_{1-x}Mn_xO_{3+\delta}$," Chem. Mater. 21, 5176-5186 (2009).
- 33 J. C. Wojdeł and J. Íñiguez, "Ab initio indications for giant magnetoelectric effects driven by structural softness," Phys. Rev. Lett. 105, 037208 (2010).
- ³⁴J. X. Zhang, Q. He, M. Trassin, W. Luo, D. Yi, M. D. Rossell, P. Yu, L. You, C. H. Wang, C. Y. Kuo, J. T. Heron, Z. Hu, R. J. Zeches, H. J. Lin, A. Tanaka, C. T. Chen, L. H. Tjeng, Y.-H. Chu, and R. Ramesh, "Microscopic origin of the giant ferroelectric polarization in tetragonal-like BiFeO₃," Phys. Rev. Lett. 107, 147602 (2011).
- 35 O. Diéguez and J. Íñiguez, "Epitaxial phases of BiMnO $_3$ from first principles," Phys. Rev. B 91, 184113 (2015).
- 36M. R. Walden, C. V. Ciobanu, and G. L. Brennecka, "Stability of epitaxial BiXO₃ phases by density-functional theory," APL Mater. 8, 081106 (2020).
- ³⁷M. R. Walden, C. V. Ciobanu, and G. L. Brennecka, "Density-functional theory calculation of magnetic properties of BiFeO3 and BiCrO3 under epitaxial strain," J. Appl. Phys. 130, 104102 (2021).
- ³⁸J. C. Fuggle, J. E. Inglesfield, and P. Andrews, *Unoccupied Electronic States*: Fundamentals for XANES, EELS, IPS and BIS (Springer, 1992), Vol. 69.
- 39T. Higuchi, W. Sakamoto, N. Itoh, T. Shimura, T. Hattori, and T. Yogo, "Valence state of Mn-doped BiFeO3-BaTiO3 ceramics probed by soft x-ray absorption spectroscopy," Appl. Phys. Express 1, 011502 (2008).
- 40 C.-S. Chen, C.-S. Tu, W. S. Chang, Y. H. Huang, P.-Y. Chen, and Y.-T. Lee, "Improved polarization switching and piezoresponse in Nd and Mn co-doped BiFeO₃ ceramics," Mater. Sci. Eng., B 269, 115180 (2021).
- ⁴¹J. B. Neaton, C. Ederer, U. V. Waghmare, N. A. Spaldin, and K. M. Rabe, "First-principles study of spontaneous polarization in multiferroic BiFeO3," Phys. Rev. B 71, 014113 (2005).
- 42J. B. Goodenough and A. L. Loeb, "Theory of ionic ordering, crystal distortion, and magnetic exchange due to covalent forces in spinels," Phys. Rev. 98, 391-408 (1955).
- $^{\mathbf{43}}$ J. B. Goodenough, "An interpretation of the magnetic properties of the perovskitetype mixed crystals $La_{1-x}Sr_xCoO_{3-\lambda}$," J. Phys. Chem. Solids 6, 287–297 (1958). 44J. Kanamori, "Superexchange interaction and symmetry properties of electron
- orbitals," J. Phys. Chem. Solids 10, 87-98 (1959).
- 45P. W. Anderson, "Antiferromagnetism. Theory of superexchange interaction," Phys. Rev. 79, 350-356 (1950).
- 46 N. V. Orlova, A. A. Shanenko, M. V. Milošević, F. M. Peeters, A. V. Vagov, and V. M. Axt, "Ginzburg-Landau theory for multiband superconductors: Microscopic derivation," Phys. Rev. B 87, 134510 (2013).
- ⁴⁷T. Moriya, "Anisotropic superexchange interaction and weak ferromagnetism," Phys. Rev. 120, 91-98 (1960).
- 48C. Michel, J.-M. Moreau, G. D. Achenbach, R. Gerson, and W. James, "The atomic structure of BiFeO₃," Solid State Commun. 7, 701–704 (1969).
- 49 M. Murakami, S. Fujino, S.-H. Lim, C. J. Long, L. G. Salamanca-Riba, M. Wuttig, I. Takeuchi, V. Nagarajan, and A. Varatharajan, "Fabrication of multiferroic epitaxial BiCrO₃ thin films," Appl. Phys. Lett. 88, 152902 (2006).
- 50N. Yang, Y. Yuan, Z. Guan, N. Zhong, W.-X. Chen, R.-J. Qi, Y.-Y. Zhang, R. Huang, X.-D. Tang, P.-H. Xiang, C.-G. Duan, and J.-H. Chu, "Structure dependence of ferroelectricity in high quality BiMnO3 epitaxial films," Phys. Rev. Mater. 3, 054402 (2019).
- ⁵¹H. Yamamoto, K. Toda, Y. Sakai, T. Nishikubo, I. Yamada, K. Shigematsu, M. Azuma, H. Sagayama, M. Mizumaki, K. Nitta, and H. Kimura, "Emergence of a cubic phase stabilized by intermetallic charge transfer in (1-x)PbVO₃-x BiCoO₃ solid solutions," Chem. Mater. **32**, 6892-6897 (2020).
- 52V. I. Anisimov and O. Gunnarsson, "Density-functional calculation of effective Coulomb interactions in metals," Phys. Rev. B 43, 7570-7574 (1991).
- 53N. Dix, J. Fontcuberta, F. Sánchez, P. Jadhav, O. Chaix-Pluchery, M. Varela, and J. Kreisel, "A phase transition close to room temperature in BiFeO3 thin films," J. Phys.: Condens. Matter 23, 342202 (2011).

- 54R. Seshadri and N. A. Hill, "Visualizing the role of Bi 6s 'Lone Pairs' in the off-center distortion in ferromagnetic BiMnO₃," Chem. Mater. 13, 2892-2899
- 55N. Mott, Metal-Insulator Transitions (Taylor & Francis, 1974).
- **56** J. F. Janak, "Proof that $\frac{\partial e}{\partial t} n_i = \varepsilon$ in density-functional theory," Phys. Rev. B **18**, 7165 (1978).
- $^{57}\mathrm{W}.$ Kohn and L. J. Sham, "Self-consistent equations including exchange and correlation effects," Phys. Rev. 140, A1133 (1965).
- 58J. P. Perdew and M. Levy, "Physical content of the exact Kohn-Sham orbital energies: Band gaps and derivative discontinuities," Phys. Rev. Lett. 51, 1884
- ⁵⁹N. Marzari and D. Vanderbilt, "Maximally localized generalized Wannier functions for composite energy bands," Phys. Rev. B 56, 12847-12865 (1997).
- 60 R. Dronskowski and P. E. Bloechl, "Crystal orbital hamilton populations (COHP): Energy-resolved visualization of chemical bonding in solids based on density-functional calculations," J. Phys. Chem. 97, 8617-8624 (1993).
- ⁶¹A. A. Mostofi, J. R. Yates, G. Pizzi, Y.-S. Lee, I. Souza, D. Vanderbilt, and N. Marzari, "An updated version of wannier90: A tool for obtaining maximallylocalised Wannier functions," Comput. Phys. Commun. 185, 2309-2310 (2014).
- 62S. Maintz, V. L. Deringer, A. L. Tchougréeff, and R. Dronskowski, "LOBSTER: A tool to extract chemical bonding from plane-wave based DFT," J. Comput. Chem. 37, 1030-1035 (2016).
- 63G. Kresse and J. Hafner, "Ab initio molecular dynamics for liquid metals," Phys. Rev. B 47, 558-561 (1993).
- 64G. Kresse and J. Hafner, "Ab initio molecular-dynamics simulation of the liquid-metal-amorphous-semiconductor transition in germanium," Phys. Rev. B 49, 14251-14269 (1994).
- 65 G. Kresse and J. Furthmüller, "Efficient iterative schemes for ab initio totalenergy calculations using a plane-wave basis set," Phys. Rev. B 54, 11169-11186
- 66G. Kresse and J. Furthmüller, "Efficiency of ab initio total energy calculations for metals and semiconductors using a plane-wave basis set," Comput. Mater. Sci. 6, 15-50 (1996).
- ⁶⁷J. P. Perdew, K. Burke, and M. Ernzerhof, "Generalized gradient approximation made simple," Phys. Rev. Lett. 77, 3865-3868 (1996).
- 68 J. P. Perdew, A. Ruzsinszky, G. I. Csonka, O. A. Vydrov, G. E. Scuseria, L. A. Constantin, X. Zhou, and K. Burke, "Restoring the density-gradient expansion for exchange in solids and surfaces," Phys. Rev. Lett. 100, 136406 (2008).
- 69 V. I. Anisimov, A. I. Poteryaev, M. A. Korotin, A. O. Anokhin, and G. Kotliar, "First-principles calculations of the electronic structure and spectra of strongly correlated systems: Dynamical mean-field theory," J. Phys.: Condens. Matter 9, 7359-7367 (1997).
- ⁷⁰S. L. Dudarev, G. A. Botton, S. Y. Savrasov, C. J. Humphreys, and A. P. Sutton, "Electron-energy-loss spectra and the structural stability of nickel oxide: An LSDA+U study," Phys. Rev. B 57, 1505-1509 (1998).
- 71 M. Cococcioni and S. de Gironcoli, "Linear response approach to the calculation of the effective interaction parameters in the LDA+U method," Phys. Rev. B 71, 035105 (2005).
- ⁷²N. A. Spaldin, "A beginners guide to the modern theory of polarization," . Solid State Chem. 195, 2-10 (2012).
- 73M. Goffinet, P. Hermet, D. I. Bilc, and P. Ghosez, "Hybrid functional study of prototypical multiferroic bismuth ferrite," Phys. Rev. B 79, 014403 (2009). ⁷⁴J. R. Teague, R. Gerson, and W. James, "Dielectric hysteresis in single crystal
- BiFeO₃," Solid State Commun. 8, 1073-1074 (1970).
- 75A. A. Belik, S. Iikubo, K. Kodama, N. Igawa, S. Shamoto, and E. Takayama-Muromachi, "Neutron powder diffraction study on the crystal and magnetic structures of BiCrO₃," Chem. Mater. 20, 3765-3769 (2008).
- 76S. Niitaka, M. Azuma, M. Takano, E. Nishibori, M. Takata, and M. Sakata, "Crystal structure and dielectric and magnetic properties of BiCrO3 as a ferroelectromagnet," Solid State Ionics 172, 557-559 (2004).
- 77A. A. Belik, N. Tsujii, H. Suzuki, and E. Takayama-Muromachi, "Magnetic properties of bulk BiCrO₃ studied with dc and ac magnetization and specific heat," Inorg. Chem. 46, 8746-8751 (2007).

- ⁷⁸A. A. Belik, S. Iikubo, T. Yokosawa, K. Kodama, N. Igawa, S. Shamoto, M. Azuma, M. Takano, K. Kimoto, Y. Matsui, and E. Takayama-Muromachi, "Origin of the monoclinic-to-monoclinic phase transition and evidence for the centrosymmetric crystal structure of BiMnO₃," J. Am. Chem. Soc. 129, 971–977 (2007).
- ⁷⁹E. Montanari, G. Calestani, L. Righi, E. Gilioli, F. Bolzoni, K. S. Knight, and P. G. Radaelli, "Structural anomalies at the magnetic transition in centrosymmetric BiMnO₃," Phys. Rev. B **75**, 220101 (2007).
- ⁸⁰A. Moreira dos Santos, S. Parashar, A. Raju, Y. Zhao, A. Cheetham, and C. Rao, "Evidence for the likely occurrence of magnetoferroelectricity in the simple perovskite, BiMnO₃," Solid State Commun. **122**, 49–52 (2002).
- 81T. Atou, H. Chiba, K. Ohoyama, Y. Yamaguchi, and Y. Syono, "Structure determination of ferromagnetic perovskite BiMnO₃," J. Solid State Chem. 145, 639–642 (1999).
- ⁸²E. Montanari, G. Calestani, A. Migliori, M. Dapiaggi, F. Bolzoni, R. Cabassi, and E. Gilioli, "High-temperature polymorphism in metastable BiMnO₃," Chem. Mater. 17, 6457–6467 (2005).
- 83P. Baettig, R. Seshadri, and N. A. Spaldin, "Anti-polarity in ideal BiMnO₃," J. Am. Chem. Soc. 129, 9854–9855 (2007).
- ⁸⁴S. Ishiwata, M. Azuma, M. Takano, E. Nishibori, M. Takata, M. Sakata, and K. Kato, "High pressure synthesis, crystal structure and physical properties of a new Ni (II) perovskite BiNiO₃," J. Mater. Chem. **12**, 3733–3737 (2002).
- ⁸⁵J. L. Ortiz-Quiñonez, D. Díaz, I. Zumeta-Dubé, H. Arriola-Santamaría, I. Betancourt, P. Santiago-Jacinto, and N. Nava-Etzana, "Easy synthesis of high-purity BiFeO₃ nanoparticles: New insights derived from the structural, optical, and magnetic characterization," Inorg. Chem. 52, 10306–10317 (2013).

- ⁸⁶V. Fruth, E. Tenea, M. Gartner, M. Anastasescu, D. Berger, R. Ramer, and M. Zaharescu, "Preparation of BiFeO₃ films by wet chemical method and their characterization," J. Eur. Ceram. Soc. **27**, 937–940 (2007).
- ⁸⁷R. Palai, R. S. Katiyar, H. Schmid, P. Tissot, S. J. Clark, J. Robertson, S. A. T. Redfern, G. Catalan, and J. F. Scott, "The beta phase of multiferroic bismuth ferrite and its beta-gamma metal-insulator transition," Phys. Rev. B 77, 014110 (2008).
- ⁸⁸T. Shimada, T. Matsui, T. Xu, K. Arisue, Y. Zhang, J. Wang, and T. Kitamura, "Multiferroic nature of intrinsic point defects in BiFeO₃: A hybrid Hartree-Fock density functional study," Phys. Rev. B **93**, 174107 (2016).
- ⁸⁹F. Gao, Y. Yuan, K. F. Wang, X. Y. Chen, F. Chen, J.-M. Liu, and Z. F. Ren, "Preparation and photoabsorption characterization of BiFeO₃ nanowires," Appl. Phys. Lett. **89**, 102506 (2006).
- 90 S. Ju, T.-Y. Cai, and G.-Y. Guo, "Electronic structure, linear, and nonlinear optical responses in magnetoelectric multiferroic material BiFeO₃," J. Chem. Phys. 130, 214708 (2009).
- ⁹¹A. Lima, "Optical properties, energy band gap and the charge carriers' effective masses of the R3c BiFeO₃ magnetoelectric compound," J. Phys. Chem. Solids 144, 109484 (2020).
- ⁹²Y. Gao, J. Wang, L. Wu, S. Bao, Y. Shen, Y. Lin, and C. Nan, "Tunable magnetic and electrical behaviors in perovskite oxides by oxygen octahedral tilting," Sci. China Mater. 58, 302–312 (2015).
- ⁹³A. Y. Borisevich, H. J. Chang, M. Huijben, M. P. Oxley, S. Okamoto, M. K. Niranjan, J. D. Burton, E. Y. Tsymbal, Y. H. Chu, P. Yu, R. Ramesh, S. V. Kalinin, and S. J. Pennycook, "Suppression of octahedral tilts and associated changes in electronic properties at epitaxial oxide heterostructure interfaces," Phys. Rev. Lett. 105, 087204 (2010).